Journal Name

Chemical Science

Dynamic Article Links ▶

ARTICLE TYPE

An Ultra-Stable Oxoiron(IV) Complex and Its Blue Conjugate Base

Jason England,[a,‡] **Jennifer O. Bigelow**[a]**, Katherine M. Van Heuvelen**[a, ‖]**, Erik R. Farquhar**[a,§]**, Marléne Martinho**[b]**, Katlyn K. Meier**[b]**, Jonathan R. Frisch**[a]**, Eckard Münck**[b]**, and Lawrence Que, Jr.**[a]

Treatment of $[Fe^{II}(L)](OTf)_2$ (**4**) , (where L = 1,4,8-Me$_3$cyclam-11-CH$_2$C(O)NMe$_2$) with iodosylbenzene yielded the corresponding S = 1 oxoiron(IV) complex $[Fe^{IV}(O(L)](OTf)_2$ (**5**) in nearly quantitative yield. The remarkably high stability of **5** ($t_{1/2} \approx$ 5 days at 25 °C) facilitated its characterization by X-ray crystallography and a raft of spectroscopic techniques. Treatment of **5** with strong base was found to
10 generate a distinct, significantly less stable S = 1 oxoiron(IV) complex, **6** ($t_{1/2}$ ~ 1.5 hrs. at 0 °C), which could be converted back to **5** by addition of a strong acid; these observations indicate that **5** and **6** represent a conjugate acid-base pair. That **6** can be formulated as $[Fe^{IV}(O)(L-H)](OTf)$ was further supported by ESI mass spectrometry, spectroscopic and electrochemical studies, and DFT calculations. The close structural similarity of **5** and **6** provided a unique opportunity to probe the influence of the
15 donor *trans* to the Fe^{IV}=O unit upon its reactivity in H-atom transfer (HAT) and O-atom transfer (OAT), and **5** was found to display greater reactivity than **6** in both OAT and HAT. While the greater OAT reactivity of **5** is expected on the basis of its higher redox potential, its higher HAT reactivity does not follow the anti-electrophilic trend reported for a series of $[Fe^{IV}(O)(TMC)(X)]$ complexes (TMC = tetramethylcyclam) and thus appears to be inconsistent with the Two-State Reactivity rationale that is the
20 prevailing explanation for the relative facility of oxoiron(IV) complexes to undergo HAT.

Introduction

Oxygen activating nonheme monoiron enzymes are responsible for catalyzing a staggeringly diverse array of biologically important oxidative transformations, despite having similar active
25 sites with the majority containing a 2-His-1-carboxylate facial triad structural motif.[1, 2] Much of this chemistry is proposed to proceed via formation of oxoiron(IV) intermediates, a notion that has been experimentally verified for several enzymes.[3-8] Spurred by a desire to understand the fundamental properties of such
30 oxoiron(IV) centers and harness their oxidative properties for synthetic purposes, a relatively large family of oxoiron(IV) complexes has been synthesized and extensively characterized, the overwhelming majority of which are intermediate-spin (S = 1).[9-11] Out of the six X-ray structures of mononuclear oxoiron(IV)
35 complexes published thus far[12-17] four are established to have an S = 1 ground state.[12-15] Furthermore, of these four structures, only the tetracarbene complex recently reported by Meyer and co-workers contains a supporting ligand with non-N donor atoms.[15] None contain O-atom donors, which are ubiquitous in nature.
40 Electronic effects on the reactivity of S = 1 oxoiron(IV) complexes have been investigated. The most significant contributions were achieved using oxoiron(IV) complexes containing a solvent occupied labile coordination site, either *cis* or *trans* to the oxo unit, allowing for exchange with various
45 ligands.[18-21] Metathesis studies of this type have been performed for a number of systems, but achieved its apotheosis in

$[Fe^{IV}(O)(TMC)(CH_3CN)]^{2+}$ (**1-CH$_3$CN**, Chart 1).[20] This is partly due to the high stability of this complex, but also because ligands *trans* to the oxo unit have been found to exert a greater influence
50 than those ligated *cis*.[21] This difference was attributed to the fact that *trans* ligands can interact with both σ- and π-type orbitals involved in the Fe=O bond but *cis* ligands cannot. Interestingly, whereas the complexes $[Fe^{IV}(O)(TMC)(X)]^+$ (**1-X**, where X = monoanion) were found to display increased reactivity in O-atom
55 transfer (OAT) with increasing electrophilicity, the reverse trend was found in hydrogen atom transfer (HAT). The latter counterintuitive 'anti-electrophilic' trend was rationalized using a Two-State Reactivity (TSR) model, which has become the prevailing explanation of HAT reactivity in low-spin oxoiron(IV)
60 systems.[22-25] In this DFT-derived model, the transition state on the S = 2 excited state potential energy surface is at significantly lower energy than its S = 1 ground state analog. Hence, the rate of reaction increases as the probability/contribution of the S = 2 excited state to reactivity increases, which is in turn inversely
65 correlated with the energy gap between the two spin states. This energy gap decreases as the donor strength of X increases; consequently, the probability/contribution of the S = 2 state increases, which is manifested in enhanced rates of reaction, thereby yielding the observed 'anti-electrophilic' trend in HAT.
70 Subsequent studies have hinted at a more complicated reaction surface for S = 1 oxoiron(IV) complexes than these simple models imply. For example, it has been found that replacing the

N-methyl substituents of TMC by benzyl groups to give $S = 1$ $[Fe^{IV}(O)(TBC)(CH_3CN)]^{2+}$ (**2**),[26] which might be expected to sterically inhibit reaction, instead resulted in HAT and OAT reactivity that is two orders of magnitude greater than that observed for **1-CH$_3$CN**.[27] The accompanying DFT study suggested that *both* HAT and OAT reactions for **2** proceeded on the $S = 2$ potential energy surface because the corresponding transition states on the $S = 1$ reaction coordinates were at prohibitively high energy. Furthermore, the energy gap for the $S = 1$ ground and $S = 2$ excited states was found to be smaller for **2** than for **1-CH$_3$CN** because of the weakened equatorial ligand field associated with TBC due to the greater steric bulk of the benzyl substituents. Therefore, relatively minor structural changes can have a large and unexpected impact upon the reactivity of oxoiron(IV) complexes. This has wide ranging implications because one must consider the structural influence of donors added to complexes such as **1-X**, in addition to their basicity. By extension, a direct comparison of the influence of donor basicity upon reactivity would require a rigid ligand framework and the use of structurally near-identical donor moieties of significantly different basicity.

During our efforts to test the scope of the TSR model, we sought to expand the series of **1-X** complexes available by displacing the solvent ligand in **1-CH$_3$CN** using a number of neutral donors (e.g. pyridine N-oxide[21]). This approach failed in all cases, presumably due to a combination of steric hindrance around the binding site and mass action (CH$_3$CN was used as the solvent). On this basis, it was reasoned that appending neutral donors to the ligand framework would promote coordination to the iron center. This supposition was tested by replacing one of the methyl substituents of TMC by a 2-pyridylmethyl group, affording the ligand TMC-py (Chart 1). This ligand was shown to be capable of supporting the desired $[Fe^{IV}(O)(TMC\text{-}py)]^{2+}$ complex (**3**),[14] in which coordination of the pyridine donor *trans* to the oxo group was confirmed by X-ray crystallography.

Herein we extend this approach by introducing a *N,N*-dimethylacetamido donor to yield 1,4,8-Me$_3$cyclam-11-CH$_2$C(O)NMe$_2$ (**L**) (Chart 1). Although there have been a handful of reports detailing the copper chemistry of this ligand,[28-32] its iron chemistry has yet to be explored. Gratifyingly, **L** was found to support an iron(II) complex, $[Fe^{II}(L)](OTf)_2$ (**4**), which could be converted to $[Fe^{IV}(O)(L)](OTf)_2$ (**5**), an oxoiron(IV) complex of unprecedented stability. Characterization of the latter by X-ray crystallography provided the first example of an oxoiron(IV) complex with an axial O-atom donor. When treated with strong base, **5** converts to its conjugate base **6**, which exhibits an unusual blue chromophore. Complexes **5** and **6** represent the first conjugate acid-base pair in oxoiron(IV) chemistry, and provide a means to assess the influence of *trans*-axial donor basicity upon
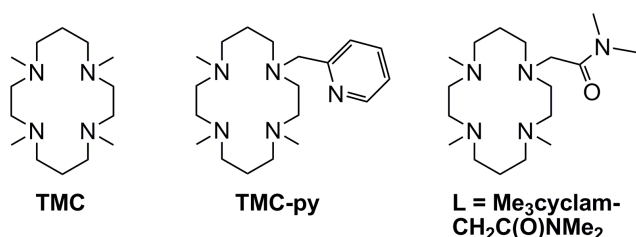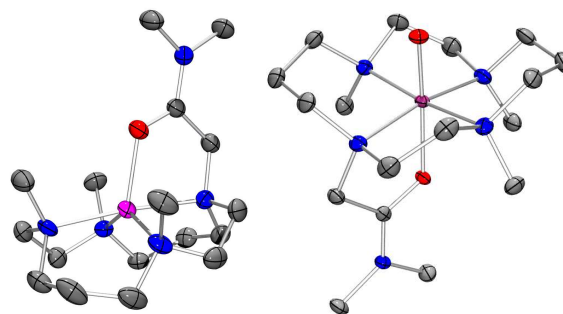

Fig. 1 Thermal ellipsoid drawings of **4** (left) and **5** (right), showing 50% probability ellipsoids. Hydrogen atoms, counterions, and solvent molecules have been omitted for clarity. Selected bond lengths are given in Table 1. Atom color scheme: C, gray; N, blue; O, red; Fe, magenta. Selected bond lengths are given in Table 1.

HAT and OAT reactivity with two complexes of similar structure.

Results and Discussion

Synthesis and Characterization of Complexes 4 and 5

Combination of the pentadentate ligand **L**[28] with Fe(OTf)$_2$(CH$_3$CN)$_2$ yielded the expected iron(II) complex $[Fe^{II}(L)](OTf)_2$ (**4**). The X-ray structure of **4** displayed a 5-coordinate geometry with $\tau = 0.51$[33] (Figure 1 left). The cyclam ring exhibits a *trans*-I configuration similar to that seen in all the previously reported X-ray structures of iron(II) TMC complexes,[27, 34] and the appended dimethylacetamido donor coordinates to the iron center via its O-atom. The associated iron-ligand bond lengths (Table 1) are typical of 5-coordinate high-spin iron(II). Furthermore, the ^{1}H NMR spectrum of this complex in CD$_3$CN (Figure S1) displays five paramagnetically shifted methyl resonances, assigned by peak integration, showing that the appended donor is not displaced by solvent and that the solid-state structure is retained in solution.

Reaction of **4** with excess iodosylbenzene gave a pale brown colored solution of a new species **5**, exhibiting an electronic spectrum with a NIR band (λ_{max} 810 nm; ε_{max} 270 M^{-1} cm^{-1}) characteristic of $S = 1$ oxoiron(IV) complexes (Figure 2, Table 2).[35] Previously, features of this type arose from ligand field transitions, with the accompanying well defined fine structure being vibronic in nature.[36, 37] Consistent with assignment of **5** as an oxoiron(IV) complex, its electrospray mass spectrum exhibited an ion fragment at $m/z = 548.2$ (Figure S12), with a mass and isotope distribution pattern in agreement with its formulation as $\{[Fe^{IV}(O)(L)](OTf)^+\}$ (calculated $m/z = 548.2$).

Complex **5** is the most stable oxoiron(IV) complex published thus far. It exhibits a half-life ($t_{1/2}$) at 25 °C in CH$_3$CN solution of approx. 5 days, which is about one order of magnitude longer than for **1-CH$_3$CN** ($t_{1/2}$ at 25 °C = 10 hrs)[18] and **3** ($t_{1/2}$ at 25 °C = 7 hrs)[14] and approximately twice that for $[Fe^{IV}(O)(N4Py)]^{2+}$ (**7**, $t_{1/2}$ at 25 °C = 60 hrs, N4Py = *N,N*-bis(2-pyridylmethyl)-*N*-bis(2-pyridyl)methyl-amine).[38] This remarkable stability allowed growth of crystals suitable for X-ray analysis. In the resultant structure (Figure 1B), the ligand retains the amide O-atom bound pentadentate *trans*-I coordination mode seen in its iron(II) precursor **4**. As a consequence, it is the only existing structure of an oxoiron(IV) complex with a supporting ligand having an

TMC

TMC-py

L = Me$_3$cyclam-CH$_2$C(O)NMe$_2$

Chart 1

oxygen donor atom.

As might be expected, oxidation of **4** to **5** is accompanied by a significant contraction of the average Fe-$N_{equatorial}$ bond lengths by *ca.* 0.1 Å (Table 1). In contrast, the axial Fe-O_{amido} shortens by
5 only *ca.* 0.02 Å, likely due to the strong *trans* effect of the oxo donor atom in the latter complex. Given this minor change in Fe-O_{amido} bond length, it is not surprising that the amide C=O and C-NMe_2 distances are virtually identical in **4** (1.267(4) and 1.309(4) Å, respectively) and **5** (1.274(2) and 1.308(2) Å, respectively).
10 These C=O and C-NMe_2 bond lengths are intermediate between values typical of single and double bonds,[39] a feature characteristic of amide functionality that stems from the resonance structure implied by canonical forms **A** and **B** (Chart 2).[40, 41] The importance of canonical form **B** is reflected by the
15 planarity of the dimethylamido N-atom in both **4** and **5**, for which the sum of its bond angles are 360˚ and the deviation of the N-atom from the plane defined by the three adjacent C-atoms is effectively zero (0.003 and 0.002 Å in **4** and **5**, respectively).

The Fe=O distance of 1.6579(13) Å seen for **5** is, within
20 experimental error, indistinguishable from those found in the other four published $S = 1$ oxoiron(IV) crystal structures (Table 1).[12-15] The average Fe-$N_{equatorial}$ distance of 2.06 Å in **5** is shorter than those of the other TMC-supported complexes **1-CH₃CN** (2.09 Å) and **3** (2.08 Å). Given that the complexes are otherwise
25 identical, these differences in average Fe-$N_{equatorial}$ distance must originate from the axial ligand. Commensurately, the most obvious difference among these three TMC oxoiron(IV) structures is the Fe-axial donor bond length, which increases in the order of **5** < **1-CH₃CN** < **3** (Table 1). The short Fe-axial
30 donor length in **5** is likely due to the greater donor strength of the dimethylacetamido donor due to some contribution from the canonical form **B** (Chart 2). However, the fact that the Fe-N_{axial} bond length in **1-CH₃CN** is 0.06 Å shorter than that of **3**, even though the acetonitrile ligand in the former is a much weaker
35 Lewis base than pyridine in the latter, suggests that steric factors may also play a role. A comparison of the three TMC-derived structures shows that the O=Fe-X_{axial} bond angle increasingly deviates from linearity in the order of **1-CH₃CN** (178.90˚) < **5** (175.57˚) < **3** (169.77°). The deviations in complexes **3** and **5**
40 may arise not only from the increasing steric bulk of the axial donor, but also from the geometric constraints of tethering a donor to the cyclam ring. Such constraints are likely to cause significant distortions of the cyclam ring and are most likely the primary origin of the observed variation of the average Fe-
45 $N_{equatorial}$ distance. Indeed, although the iron center sits close to the mean plane of the N_{TMC} donors in **1-CH₃CN**, **3** and **5** (it only deviates towards the oxo donor by 0.033 Å in **1-CH₃CN** and **5**, and by 0.071 Å in **3**), the average deviation of the N_{TMC} atoms themselves from this plane of 0.174 Å in **5** is much larger than in
50 either **3** or **1-CH₃CN** (0.027 and 0.004 Å, respectively). In any case, the availability of a third structure for an
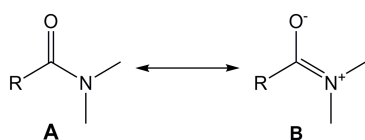
Chart 2

Table 1 Comparison of selected structural parameters for published $S = 1$
55 oxoiron(IV) and related complexes

Complex	Bond Lengths (Å)			O=Fe-X_{axial} bond angle (°)
	Fe=O	Avg. Fe-$N_{equatorial}$ donor	Fe-X_{axial}	
4	-	2.164	2.000(2)	-
5	1.6579(13)	2.0605	1.9807(12)	175.57(6)
5 (DFT)	1.646	2.103	2.024	173.79
5 (EXAFS)[a]	1.63	2.04		-
6 (DFT)	1.667	2.102	1.944	177.31
6 (EXAFS)[a]	1.67	2.03		-
1-CH₃CN[b]	1.646(3)	2.091	2.058(3)	178.9(1)
1-CH₃CN (DFT)[b]	1.640	2.133	2.099	-
3[c]	1.667(3)	2.083	2.118(3)	169.77(13)
3 (DFT)	1.649	2.136	2.135	-
7[d]	1.639(5)	1.957	2.033(8)	178.6(3)
8[e]	1.661(3)	2.010	2.105(4)	176.65(17)

[a] The resolution of this technique is not sufficient to distinguish between N_{cyclam} and O_{amide} scatterers. [b] From reference 12. [c] This X-ray structure displayed disorder due to co-crystallization of enantiomers and only the data for the major enantiomer is presented herein; from reference 14. [d] **7** =
60 [$Fe^{IV}(O)(N4Py)$]²⁺ (N4Py = *N,N*-bis(2-pyridylmethyl)-*N*-bis(2-pyridyl)-methylamine); from reference 13. [e] **8** = [$Fe^{IV}(O)(L^{NHC})(EtCN)$]²⁺ ($L^{NHC}$ = 1,3,6,9,12,14,17,20-octaazapentacyclo[18.2.1.1³,⁶.1⁹,¹².1¹⁴,¹⁷]-hexacosa-4,10,15,21-tetraene-23,24,25,26-tetraylidene) from reference 15.

[$Fe^{IV}(O)(TMC)(X)$]ⁿ⁺ complex with a neutral axial ligand X
65 allows us to discern a trend that emerges from these data. The progressive shortening of the axial ligand bond from **5** to **1** to **3** parallels an increase in the lifetime of the oxoiron(IV) unit, suggesting that a more strongly bound neutral axial ligand stabilizes the $Fe^{IV}=O$ unit. In contrast, when the axial ligand X is
70 monoanionic, the opposite trend in thermal stability is observed, with the more basic ligand affording a shorter lived oxoiron(IV) complex.[35] These opposing trends reveal complexities in the chemistry of nonheme oxoiron(IV) complexes that have yet to be understood.

75 **Treatment of Oxoiron(IV) Complex 5 with Strong Base**

Interestingly, treatment of **5** with excess tetraalkylammonium hydroxide or methoxide instantaneously yielded a new species **6** that is significantly less stable. At 0 °C, it decayed over a period of 1.5 hr, representing a difference in thermal stability of about
80 three orders of magnitude. Complex **6** not only exhibited NIR features characteristic of an $S = 1$ oxoiron(IV) complex, yet distinct from those of **5**, but also a band centered at 588 nm (ε_{max} = 460 M^{-1} cm^{-1}) that gives this species its unusual blue color (Figure 2). Notably, there are significant optical differences
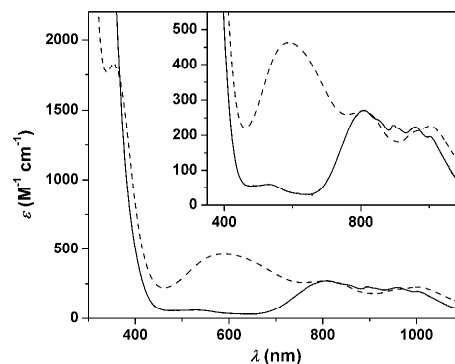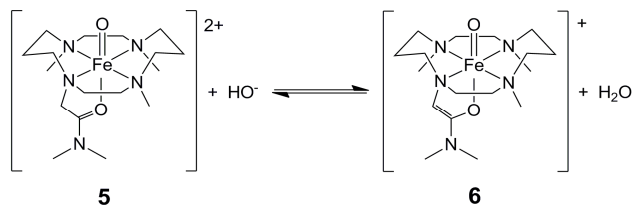85

Fig. 2 The electronic spectra of **5** (solid line) at 25 °C and **6** (dashed line) at -40 °C in CH₃CN. Inset: expansion of the visible and near-IR regions.

Scheme 1

between **6** and $[Fe^{IV}(O)(TMC)(OH)]^+$ (**1-OH**, Table 2), for which no visible absorption features were observed,[35] which suggests that hydroxide/alkoxide does not coordinate to the metal center in **6** and instead performs an alternate function. Neutralization of the hydroxide used to generate **6**, by addition of an equimolar quantity of perchloric acid, regenerated the parent complex **5** in approximately 80% yield, suggesting that **5** and **6** simply comprise a Bronsted conjugate acid-base pair. This notion is strongly supported by the electrospray mass spectrum of **6** (Figure S13), which is dominated by an ion fragment with $m/z = 397.9$ and an isotope distribution pattern consistent with its assignment as $\{[Fe^{IV}(O)(L)] - H\}^+$ (calculated $m/z = 398.2$), the product of deprotonation of **5**. Given that the most probable site of deprotonation in **5** is the relatively acidic methylene linker of the pendant donor arm (Scheme 1), **6** is formulated as $[Fe^{IV}(O)(L-H)](OTf)$. This assignment is supported by the spectroscopic and DFT studies detailed in subsequent sections.

Spectroscopic Comparison of 5 and 6

Spectroscopic features show **5** and **6** to be closely related, but distinct oxoiron(IV) complexes. For instance, the ^{1}H NMR spectra of **5** and **6** (Figure 3) both show a set of resonances heavily skewed towards negative chemical shifts (the reverse is true of the iron(II) starting complex **4**), which is typical of $S = 1$ oxoiron(IV) complexes.[13, 42] Most importantly, these two spectra are composed of a set of resonances distinct from one another,
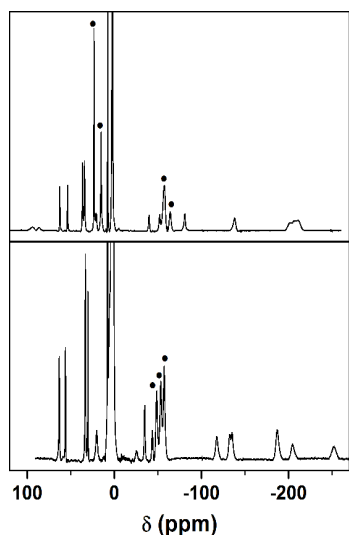

Fig. 3 ^{1}H NMR spectra **5** (top) and **6** (bottom) in CD_3CN at -40 °C with methyl resonances indicated with dots. Acquisition time = 0.064 sec.; relaxation delay = 0.03 sec.; line broadening factor = 30 Hz. Comprehensive peak assignments are provided in the Electronic Supplementary Information.

consistent with the presence of a single C_1-symmetric species. (Full spectral assignments, plus some information on how they were arrived at, are detailed in the Electronic Supplementary Information.) This indicates that treatment of **5** with base results in complete conversion to **6**. On the basis of peak integration, it is clear that the spectrum of **5** contains paramagnetically shifted resonances corresponding to five methyl groups, thereby confirming continued pentadentate coordination of the supporting ligand. In contrast, only paramagnetically shifted peaks belonging to the three methyl substituents of the cyclam ring are observed in the spectrum of **6**, presumably because the resonances corresponding to the N,N-dimethylacetamido donor have shifted into the 0 – 10 ppm region, where there are intense peaks associated with the solvent, NBu_4^+, H_2O and PhI. The reduced chemical shift of the methyl substituents in the latter is suggestive of decreased spin density on the NMe_2 unit in **6** relative to **5**. Such a scenario might be expected due to decreased interaction of the NMe_2 group with the iron center in the enolate-like structure of the former, presumably because of the reduced importance of canonical form **B** in Chart 2, consistent with the formulation of **6** provided in Scheme 1.

Mössbauer studies corroborate the ^{1}H NMR findings. The zero field Mössbauer spectrum of **5** recorded at 4.2 K exhibits a doublet representing ca. 93% of the iron with quadrupole splitting $\Delta E_Q = 1.10$ mm/s and isomer shift $\delta = 0.13$ mm/s (Figure 4A). Applied magnetic fields, B, elicit magnetic hyperfine interactions with parameters typical of $S = 1$ $Fe^{IV}=O$ complexes (Figure 4B-D). We have analyzed the data for **5** using the $S = 1$ spin Hamiltonian,

$$\mathcal{H}_e = D\left(\hat{S}_z^2 - 2/3\right) + E\left(\hat{S}_x^2 - \hat{S}_y^2\right) + \beta\hat{\boldsymbol{S}} \cdot \mathbf{g} \cdot \mathbf{B} + \hat{\boldsymbol{S}} \cdot \mathbf{A} \cdot \hat{\boldsymbol{I}} - g_n\beta_n\mathbf{B} \cdot \hat{\boldsymbol{I}} + \mathcal{H}_Q$$

$$\mathcal{H}_Q = \left(eQV_{zz}/12\right)\left[3\hat{I}_z^2 - 15/14 + \eta\left(\hat{I}_x^2 - \hat{I}_y^2\right)\right] \quad (1)$$

where all symbols have their conventional meanings. Within resolution, the zero-field splitting (ZFS) tensor, described by the parameters D and E, was found to be axial ($E = 0$). The value of D was obtained by fitting the variable field data obtained at 4.2 K, for which the splitting along molecular direction i is roughly linear in (A_i/D), and taking into account that the 100 K/8.0 T spectrum is essentially independent of D. The resulting value $D = 27 \pm 2$ cm^{-1} for **5** is typical of oxoiron(IV) complexes of the TMC ligand.[35]

Obtaining Mössbauer spectra of **6** was not straightforward due to bleaching of the blue chromophore of **6** and reformation of **5** (established by Mössbauer spectroscopy) upon freezing of acetonitrile solutions of **6**. This problem was circumvented by using toluene solutions of tetraoctylammonium hydroxide[43] in place of tetrabutylammonium hydroxide to minimize the amount of water present in the system. This necessitated use of the more lipophilic solvent, butyronitrile. The Mössbauer spectrum of an unbleached sample of **6** confirmed formation of a new iron(IV) complex in 86% yield with ≤5% residual **5** and a ferric impurity making up the balance. In zero field we observed a doublet with $\Delta E_Q = 0.51$ mm/s and $\delta = 0.12$ mm/s (Figure 4E). While the δ values of **5** and **6** are the same, their ΔE_Q values are quite distinct. The ΔE_Q observed for **6** is in the range associated with $[Fe^{IV}(O)(TMC)(X)]^+$ (**1-X**) complexes with basic axial ligands
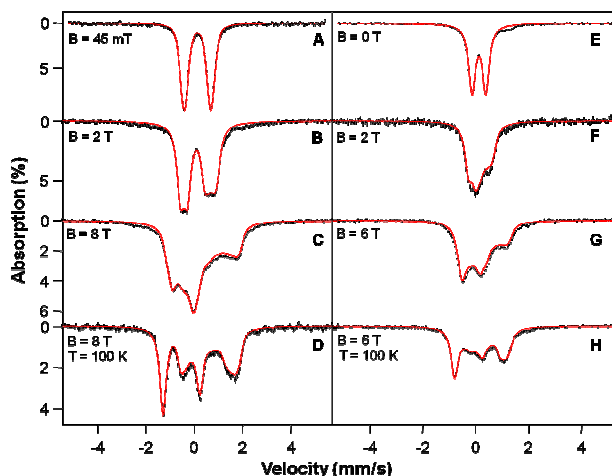
Fig. 4 Mössbauer spectra of **5** (**A-D**) and **6** (**E-H**) recorded at 4.2 K (**A-C**, **E-G**) and 100 K (**D**, **H**) in applied fields as indicated. Red lines are simulations for **5** (~93% of Fe) and **6** (~ 86% of Fe), obtained by using Eq. 1 and the parameters listed in Table 2. The sample for **6**, has a ~10% likely diferric contaminant with $\Delta E_Q \approx 0.51$ mm/s and $\delta \approx 0.52$ mm/s.

such as SCN[-], NCO[-] and N$_3$[-] (**1-NCS**, **1-NCO** and **1-N$_3$**, respectively; Table 2),[35] but is significantly larger than that reported for **1-OH**, which supports the notion that formation of **6** is unlikely due to the displacement of the dimethylacetamide axial ligand. From the analysis of the applied field spectra we obtained the parameters listed in Table 2.

The resonance Raman spectra of complexes **5** and **6** exhibit ν(Fe=O) of 833 and 823 cm^{-1} (Figure 5), respectively. In accordance with expectations from Hooke's Law for a diatomic oscillator, these features downshift by 35 and 36 cm^{-1} upon ^{18}O-labelling of **5** and **6**, respectively. That the ν(Fe=O) of **6** is 10 cm^{-1} lower in energy than that for **5** implies a slight weakening of the Fe=O bond, consistent with the expected greater donor strength of the anionic enolate donor in the former relative to the neutral *N,N*-dimethylacetamide donor in the latter. Of particular note is that the ν(Fe=O) in **6** is not only resonance enhanced by excitation at 407 nm, as seen for other TMC-ligated oxoiron(IV) complexes, but also at 568 nm. (In fact, the greater enhancement in intensity is observed using light with the latter wavelength.) This observation indicates that the electronic transition in **6** centered at 588 nm, and possibly also that at 352 nm, involve occupation of orbitals associated with the Fe=O unit (*vide infra*). The greater enhancement of the ν(Fe=O) mode observed with 568-nm excitation likely arises from the photoinstability of the complex upon near-UV irradiation, as noted previously for other Fe^{IV}=O complexes we have studied.[14, 35]

The Fe K-edge X-ray absorption spectra of **5** and **6** exhibit virtually superimposable normalized XANES regions (Figure 6A), with respective edge energies of 7125.91 and 7125.83 eV and pre-edge energies of 7114.18(1) and 7114.14(1) eV (Table S3), suggesting that the differences in iron(IV) environment inferred from Mössbauer spectroscopy do not significantly impact the transitions comprising both the rising K-edge and the near-edge regions of the XAS spectrum. Both the edge and pre-edge energies are in line with values obtained previously for other oxoiron(IV) complexes (Table 2).[35, 44] Indeed, the only notable difference between the XANES spectra of these two iron(IV)

species is that the area of the pre-edge feature is moderately larger for **5** than that of **6** (30.4 and 23 units, respectively). The intensity of this feature, which originates from 1s-to-3d transitions at the iron center, generally reflects the extent to which distortion from centrosymmetry facilitates 4p mixing into the 3d orbitals and increases the probability of transition. Hence, the smaller pre-edge area of **6** reflects a more centrosymmetric coordination environment, stemming from stronger coordination by the pendant donor. The larger pre-edge area and ΔE_Q values for **5** are in line with the correlation previously established by Jackson and co-workers,[35] which indicates that the magnitude of pre-edge area and ΔE_Q scale proportionally to one another, as they both reflect the symmetry of the electron density around the iron center.

In good agreement with its X-ray structure, EXAFS analysis of **5** yielded a best fit with 5 O/N scatterers at 2.04 Å, attributable to the 5 donor atoms of the ligand, and a further O/N scattering atom at 1.63 Å that corresponds to the Fe=O unit (Figure 6B, Tables S4 and S5). A similar best-fit EXAFS analysis is obtained for **6**, consisting of 5 O/N scatterers at 2.03 Å and a single O/N scatterer at 1.67 Å (Table S6). This data serves to further confirm that the Fe=O moiety is retained in **6**, with the slight elongation in its length due to the increased basicity of the *trans*-oriented donor. Attempts to resolve a shortened Fe–O$_{amide}$ distance in the EXAFS of **5** and **6** by splitting the principal O/N shell were unsuccessful, on the basis of a poorer overall goodness of fit. However, it should be noted that the Debye-Waller factor associated with this shell in **6** is considerably larger than that of its precursor **5**, which presumably reflects greater static disorder in the range of bond lengths comprising this shell and is consistent with a decreased Fe–O$_{amide}$ distance in **6**.

Taken together, the spectroscopic data presented here show that **5** and **6** fit well into the series of [Fe^{IV}(O)(TMC)(X)] complexes that have been characterized over the past decade (Table 2).[35] Complex **5** represents only the third complex in the series where X is a neutral ligand. Complex **6** is the conjugate
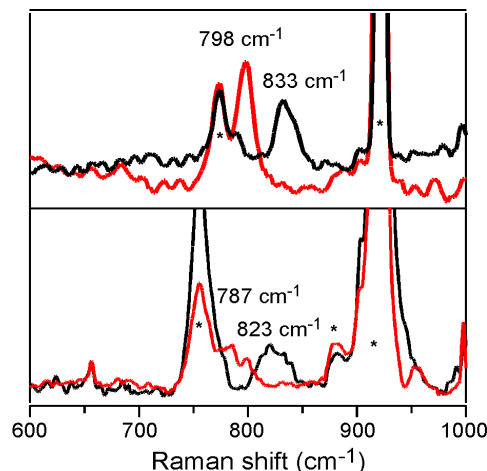

Fig. 5 Top: resonance Raman spectra of **5** (black line) and its ^{18}O-labeled isotopomer (red line), recorded in frozen CH$_3$CN solution with samples mounted on a brass cold finger (λ_{ex} = 407 nm, power = 20 mW). Bottom: resonance Raman spectra of **6** (black line) and its ^{18}O-labeled isotopomer (red line) obtained in CH$_3$CN solutions at -20 °C (λ_{ex} = 568.2 nm, power = 90 mW). Asterisks designate features from the CH$_3$CN solvent.

Table 2 Spectroscopic properties of selected TMC-based oxoiron(IV) complexes

Complex	λ_{max}, nm (ε_{max}, M^{-1} cm^{-1})	ν(Fe=O) (cm^{-1})	D (cm^{-1})	$A_{x,y,z}/g_n\beta_n$ (T)^a	ΔE_Q (mm/s)	η	δ (mm/s)	E_0 (eV)	Pre-edge Area^b
5	810 (270)	833	27(2)	-22(2), -22(2), -3(2)	+1.10(1)	~0	0.13(1)	7125.9	30.4(3)
5 (*DFT*)				*-21.7, -21.5, -4.8^a*	*+1.07*	0.18	*0.145*		
6	352 (1830), 588 (460), 806 (270), 1005 (230)	823	29(2)	-23.5 (2), -23.5 (2), -2 (2)	0.51(1)	0.4	0.13(1)	7125.8	23
6 (*DFT*)				*-21.5, -21.8, -4.7^a*	*-0.22*	0.78	*0.15*		
1-CH$_3$CN^c	282 (10000), 824 (400)	839	29	-23, -18, -3	1.23	0.5	0.17	7124.5	32.8
1-OH^d	830(100), 1060 (110)	n.d.	31	-22, -22, -2	0.16	-3.0	0.15	7125.4	21.7
1-NCS^d	387 (3500), 850 (200), 1010 (130)	820	30	-24, -20, -4	0.60	0.2	0.16	7125.4	29.1
1-NCO^d	350 (3100), 845 (200), 1010 (170)	822	31	-23, -23, -5	0.42	0.1	0.16	7125.3	30.5
1-N$_3$^{d}	407 (3600), 850 (130), 1050 (110)	814	29	-24, -20, -5	0.70	0.1	0.17	7125.3	29.6
3^e	834 (260)	826			1.08		0.18	7124.0	34
9^d	460 (1300), 570 (1100), 860 (230)	n.d.	35	-23, -22, -5	-0.22	0	0.19	7125.1	20.0

^{a} Calculated A-tensor was obtained by taking the experimentally determined A_{iso} = -19.4 T and adding the spin-dipolar term obtained from DFT. ^{b} Weighted pre-edge areas scaled to values expected for pure oxoiron(IV) complex, which assumes that other impurities present do not contribute significantly to the pre-edge. ^{c} From references 12 and 35. ^{d} [Fe^{IV}(O)(TMC)(X)]$^+$ (**1-X**), where X = OH, NCS, and N$_3$ and [Fe^{IV}(O)(TMCS)]$^+$ (**9**); data from reference 35. ^{e} From reference 14.
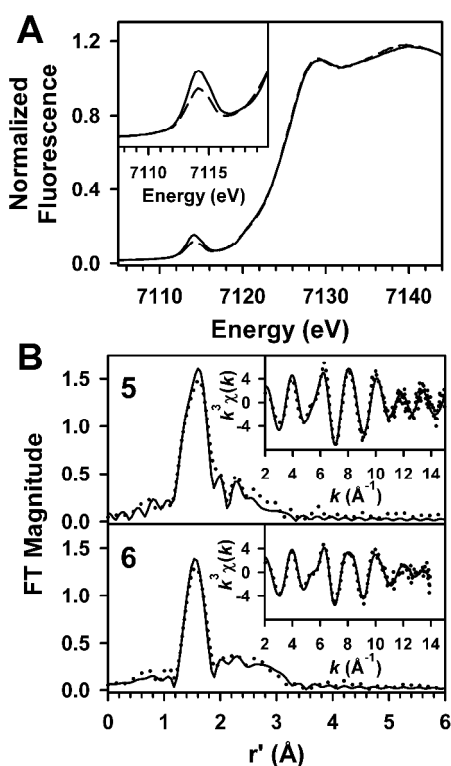

Fig. 6 (**A**) Comparison of Fe K-edge XANES spectra and pre-edge features (inset) of **5** (solid line) and **6** (dashed line). (**B**) Fits to the Fourier transforms of the Fe K-edge EXAFS data ($k^3\chi(k)$) and unfiltered EXAFS spectra ($k^3\chi(k)$), insets, for **5** and **6**. Experimental data is shown with dotted lines, while fits are shown with solid lines. Fourier transformation ranges are as follows: k = 2.0 – 15 Å^{-1} (**5**) and k = 2.0 - 14.0 Å^{-1} (**6**). Fit parameters are shown in bold italics in Table S5 and S6 of the Electronic Supplementary Information.

base of **5**, where one of the relatively acidic protons on the methylene linker of the pendant donor arm is abstracted by the addition of base. This step is postulated to convert the neutral dimethylacetamide ligand into an enolate anion as shown in Scheme 1. When the spectroscopic properties of **6** are compared with those of the other complexes in Table 2, the ν(Fe=O) and ΔE_Q values of **6** closely resemble to those of **1**-NCS and **1**-NCO, while the XAS pre-edge area of **6** approaches that of **1**-OH. These comparisons suggest that the axial donor of **6** has a basicity intermediate between NCS$^-$/NCO$^-$ and hydroxide.

DFT Studies

DFT calculations using the B3LYP/6-311g functional and basis set were carried out to gain further insight into the differences in electronic structure between **5** and **6**. Given the tendency of DFT to overestimate metal-ligand bond lengths, the agreement between the DFT geometry optimized and X-ray structures of **5** is excellent, with the calculated Fe=O and the average Fe-N/O$_{TMC}$ distances being *ca.* 0.012 and 0.04 Å, respectively, longer than the experimental values (Figure S16, Table 1). DFT analysis of the proposed structure of **6** yields a geometry optimized structure in which the expected enolate-like character is reflected by respective changes in the C–C(O)NMe$_2$, C=O, and C–NMe$_2$ bonds, from 1.515, 1.296 and 1.328 Å in **5** to 1.369, 1.360 and 1.375 Å in **6**. The negative charge on the dimethylacetamido oxygen donor atom in **6** leads to a shortening of the Fe-O$_{amide}$ bond by *ca.* 0.08 Å to 1.944 Å and an increase in the Fe=O distance by ca. 0.02 Å to 1.667 Å, but crucially does *not* perturb the average Fe-N$_{TMC}$ distance, which differs by only 0.001 Å between **5** and **6**. Hence, any differences between the reactivity and spectroscopic properties of these two species can be attributed solely to the change in the axial donor *trans* to the Fe^{IV}=O. It should be noted that the changes in the Fe-donor atom bond lengths predicted by DFT are consistent with the structural parameters obtained by EXAFS (Tables 1 and S4-S6).

The calculated and experimental Mössbauer parameters for **5** agree very well. In particular, the calculated spin dipolar part of the A-tensor and the electric field gradient (EFG) tensor have their largest component along z, in agreement with the Mössbauer analysis of eq 1 (the zero-field splitting of Fe^{IV}=O complexes is generally axial around the Fe=O bond, the chosen z axis.). The calculated A-tensor of **6** also agrees well with the experimental data. However, ΔE_Q differs from the experimental data by 0.7 mm/s. Close inspection of the output DFT files of **5** and **6** did not reveal any particular feature that allowed us to identify the source for the difference in the calculated ΔE_Q's of **5** and **6**. We note that for **6** the calculated spin-dipolar part of **A** for **6** agrees well with the data, and this part is proportional to the valence part of the EFG. We thus would expect that the *valence* part of the EFG is
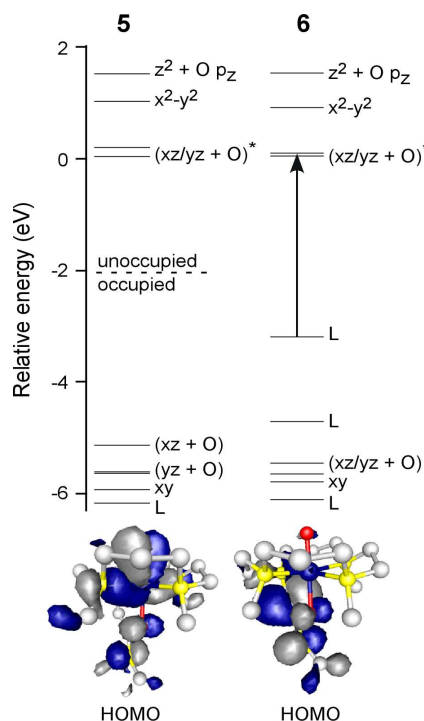
Fig. 7 Top: spin-down molecular orbitals of **5** and **6** generated using the single-parameter PBE0 functional. For comparison, orbital energies are plotted relative to the spin-down LUMO. The electronic transition that gives rise to the 588 nm optical feature of **6** is marked with an arrow. Bottom: isosurface plots of the spin-up HOMOs of **5** (left) and **6** (right).

well represented by the calculations, and the deviations might be rooted in covalecy effects. We note that calculated ΔE_Q values often differ substantially from experimental data, for reasons not well understood, and thus the disagreement for **6** is thus not surprising; in fact the good agreement for **5** may be a bit fortuitous.

In order to investigate the origin of the 588 nm feature in the UV-visible spectrum of **6**, spin-unrestricted time-dependent DFT (TD-DFT) studies of **5** and **6** were conducted using the PBE0 functional. These calculations gave rise to the frontier molecular orbital energy diagrams for **5** and **6** shown in Figure 7, which can be used to understand the spectroscopic differences between **5** and **6**. In the case of **5**, the spin-up (α) and spin-down (β) highest occupied molecular orbitals (HOMO) are primarily (Fe d_{xz} + O p_x) in character and the occupied ligand-derived MOs are lower in energy. Upon deprotonation of the methylene group of the pentadentate ligand **L**, the ligand-based MOs are destabilized and become the α and β HOMOs in **6** (Figure S18). The TD-DFT generated UV-visible spectrum of **5** is shown in Figure 8. Examination of the electron density difference map (EDDM) corresponding to state i reveals that the near-IR band at 810 nm can be assigned as a (Fe d_{yz})-to-(Fe d_{x2-y2}) ligand-field transition, while state ii arises from an oxo-to-iron charge transfer transition. This assignment is corroborated by the resonance Raman data presented in Figure 5, which demonstrates that laser excitation into the near-UV feature results in resonance-enhancement of the ν(Fe=O) vibration. It should be noted that electronic spectra of this type, incorporating ligand field transitions at ~800 nm and an intense charge transfer band in the near-UV spectral region, are characteristic of

$[Fe^{IV}(O)(TMC)(X)]^+$ complexes.[35] Computational results indicate that acetamide-to-Fe=O transitions should occur at high energy (> 33,000 cm^{-1}), outside of our experimental detection limit.

Consistent with experimental data, the calculated UV-visible spectrum of **6** exhibits multiple electronic transitions in the visible region that are absent in **5**. As is typical of $S = 1$ oxoiron(IV) complexes, the lowest energy feature in the near IR region (state iii) is predominantly ligand field in character. Likewise, the intense band in the near-UV region of **6** (state vii) may be assigned as an oxo-to-iron charge transfer transition. However, in contrast to the analogous spectral features observed in **5**, the dimethylacetamido moiety contributes to each of these electronic transitions by acting as an electron donor. Similarly, the EDDM associated with state v indicates that the unique 588 nm feature in **6** is a ligand-to-iron charge transfer transition in which electron density from the enolate-like moiety is donated to the vacant β (Fe d_{yz}+O p_y)* orbital. The destabilization of the ligand-based orbitals results in a red-shift of acetamide-to-iron transitions relative to **5** and gives rise to the novel electronic absorption features observed for **6**.

Taken as a whole, the assignment of the features of the electronic spectra of **5** and **6** are analogous to those previously described for TMC-supported complexes **1-X** (X = CH$_3$CN, SCN$^-$, NCO$^-$ and N$_3^-$), with intense oxo-to-iron charge transfer
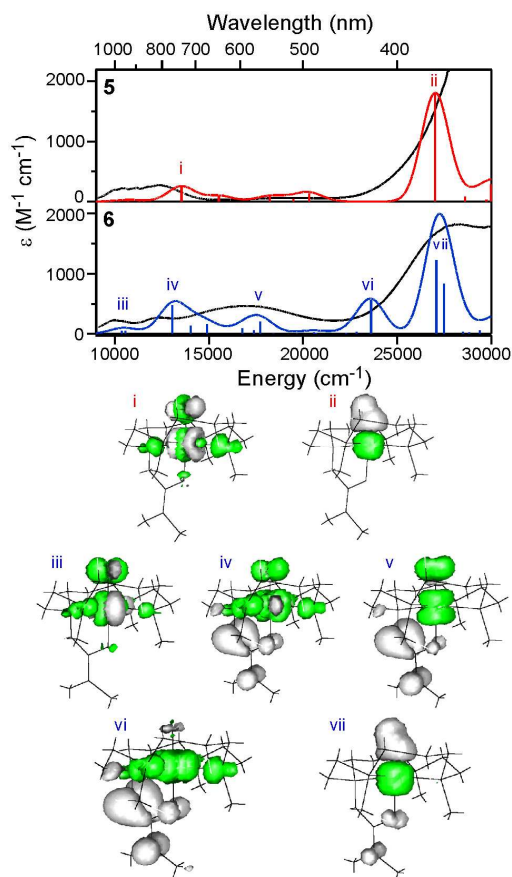

Fig. 8 Top: calculated (PBE0) and experimental electronic absorption spectra of **5** and **6**. The intensity of the simulated spectrum of **6** was scaled by a factor of 2/3 to facilitate comparison with experimental data. Bottom: electron density difference maps (EDDMs) illustrating the loss (grey) and gain (green) of electron density.

transitions located in the UV region and ligand field transitions in the near-IR region (Table 2).[36, 37] Additionally, the pseudohalide-ligated oxoiron(IV) complexes **1-NCS**, **1-OCN** and **1-N₃** display moderately intense charge transfer bands in the near-UV that were assigned as being pseudohalide-to-Fe=O in origin.[35] The HOMOs of these pseudohalides are quite simply at lower energy than those of the enolate-like donor in **6**, so these charge transfer transitions occur at higher energy. It should be noted that an oxoiron(IV) complex with a chromophore centered in the visible region is not without precedent, with the [Fe^{IV}(O)(TMCS)]$^+$ (**9**) complex displaying two such bands at 460 and 570 nm that also render this complex blue and are presumed to originate from thiolate-to-Fe=O transitions.[45]

Electrochemistry and Reactivity

The addition of a conjugate acid-base pair to the family of TMC-ligated nonheme oxoiron(IV) complexes provides a unique opportunity to compare their redox behavior with that of other members of the family. Previous studies of four [Fe^{IV}(O)(TMC)X] complexes (X = NCCH₃, O₂CCF₃, N₃, SR) by cyclic voltammetry in MeCN showed an irreversible reduction peak for each of these complexes in the range of -0.3 – -1 V *vs* the ferrocenium/ferrocene redox couple (Fc$^{+/o}$).[20] The relative order of $E_{p,c}$ values obtained was rationalized by the electron donating properties of the axial donor, X. Not surprisingly, potentials spanning the same range were observed in cyclic voltammetric measurements of **3** (Figure S19), **5** and **6** (Figure 9) and provide additional points that can be used to make correlations with oxidative reactivity data.

Cyclic voltammetry of **3** in MeCN at room temperature revealed a reduction peak at -0.48 V *vs* Fc$^{+/o}$, similar to that of [Fe^{IV}(O)(TMC)(O₂CCF₃)]$^+$. In the case of **5**, however, two comparably sized reduction peaks were observed: one at -0.63 V
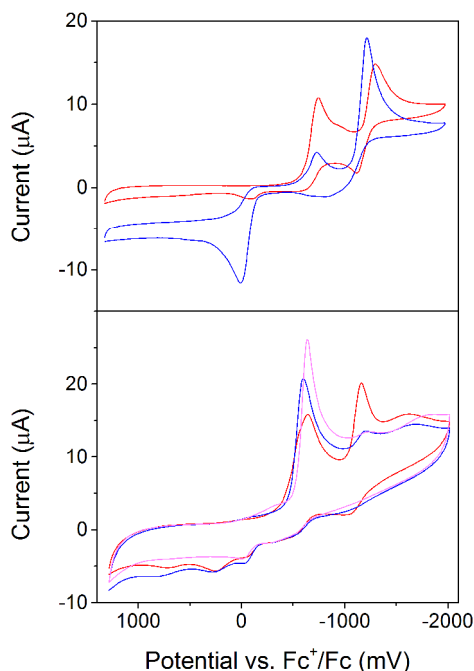

Fig. 9 Cyclic voltammograms of **5** in CH₃CN, scan rate: 100 mV/s. Top: before (red) and after (blue) the addition of 1.4 eq. NBu₄(OH) at -40 °C. Bottom: before (red) and after the addition of 0.1 eq. (blue) and 0.2 eq. pyridinium triflate (magenta) at room temperature.

and a second at -1.16 V (Figure 9 bottom, red line). At -40 °C, **5** (Figure 9, top) can be compared to **6** by the addition of Bu₄N(OH) to a solution of **5** (Figure 9 top, blue line); this resulted in an increase in the current of the lower potential peak and the suppression of the higher potential peak. On the other hand, the addition of pyridinium triflate increased the intensity of the current associated with the $E_{p,c}$ peak at -0.63 V and suppressed the $E_{p,c}$ peak at -1.16 V (Figure 9 bottom). To rationalize the observed behavior above, we attribute the feature at -0.63 V to the reduction of **5** and the feature at -1.16 V to the reduction of **6**, which is supported by the effects of adding base or acid. The appearance of the second reduction wave in the cyclic voltammetry of **5** suggests that **6** can be generated spontaneously. We propose that the reduction of **5** produces a highly basic Fe^{III}-O$^-$ moiety, which in turn deprotonates some remaining **5** in solution to form **6**. Protonation of the 1-e$^-$-reduced Fe^{III}-O$^-$ species (formed from the reduction of **5**) by added pyridinium triflate prevents **6** from being formed, thus decreasing the current for the second peak at -1.16 V.

The oxidative reactivity of **3**, **5**, and **6** was compared with that of the [Fe^{IV}(O)(TMC)(X)] series (X = NCMe, O₂CCF₃, N₃, and SR) studied by Sastri *et al.* at 0 °C.[20] For **3** and **5**, the reaction with PPh₃ produced OPPh₃ in 93% and 90% yield, while the reaction of **6** with PMePh₂ produced OPMePh₂ in 83% yield. All iron(IV)-oxos reacted with 1,4-cyclohexadiene to produce benzene in 60-80% yield. The second order rate constant, k_2, of **3** for oxygen atom transfer (OAT) to PPh₃ was found to be 3.8 M^{-1} s^{-1}, comparable to that for **1-CH₃CN**. However, the OAT value for **5** was 0.19 M^{-1} s^{-1}, more than an order of magnitude smaller than for **1-CH₃CN**, and that for **6** was too slow to be distinguished from its self-decay. In order to obtain a more quantitative reactivity comparison of **5** and **6**, we carried out OAT reactivity studies with PMePh₂ and found **6** to react about 20-fold more slowly than **5** (Table 3). This order of decreasing OAT rates appears to correlate with the increasing basicity of the axial ligand, as noted previously for the [Fe^{IV}(O)(TMC)(X)] series studied by Sastri *et al.*[20] This trend is visually demonstrated by a plot of log k_2 *vs* $E_{p,c}$ (Figure 10 top) where the data points for **3**, **5**, and **6** lie close to the trendline defined only by data points associated with the [Fe^{IV}(O)(TMC)(X)] series studied by Sastri *et al.*, reflecting the decreasing electrophilicity of the Fe^{IV}=O unit with an increasingly basic axial ligand. A similar linear correlation between OAT rates and redox potential noted for a series of complexes supported by pentadentate N5 ligands reinforces this conclusion.[46, 47]

In contrast, **5** and **6** exhibit a much smaller difference in the rates of the H-atom transfer (HAT) reactions. The k_2 value for the reaction of **5** with 1,4-cyclohexadiene (CHD) is only twofold larger than for **6**; these values are in turn an order of magnitude smaller than those of **1-CH₃CN** and **3** (Table 3). However, unlike for OAT, the HAT rates of all [Fe^{IV}(O)(TMC)(X)] complexes do not display a consistent trend with redox potential (Figure 10, bottom). In the subset of [Fe^{IV}(O)(TMC)(X)] complexes studied by Sastri *et al.*,[20] an anti-electrophilic trend was observed, where the HAT rate constant decreased with increasing redox potential. A similar trend was found in another study of Fe^{IV}(O) complexes of a different tetragonal N4 ligand L^{8}py₂ (L^{8}py₂ = *N,N'*-bis(2-pyridylmethyl)-1,5-diazacyclooctane) where the axial ligand trans

Table 3 Rate constants and $E_{p,c}$ values *vs* Fc$^+$/Fc in CH$_3$CN for tetraalkylcyclam-ligated oxoiron(IV) complexes

Complex	$t_{1/2}$	k_2 [M^{-1} s^{-1}] in CH$_3$CN, 0 °C			$E_{p,c}$ (V *vs* Fc$^+$/Fc)	
		CHD^a	PPh$_3$	PMePh$_2$	RT^e	-40 °C
1-CH$_3$CN^b	10 hrs (25 °C)	0.12	5.9	-	-0.32	-
3	7 hrs^c (25 °C)	0.22(1)	3.8	-	-0.48	-
5	5 days (25 °C)	0.037(2)	0.19	5.9(3)	-0.63	-0.74
6	~ 1.5 hrs (0 °C)	0.016(1)	<0.004^d	0.32(2)	-1.16	-1.23

^{a} 1,4-cyclohexadiene. ^{b} From reference 18. ^{c} From reference 14. ^{d} Indistinguishable from self-decay. ^{e} room temperature.
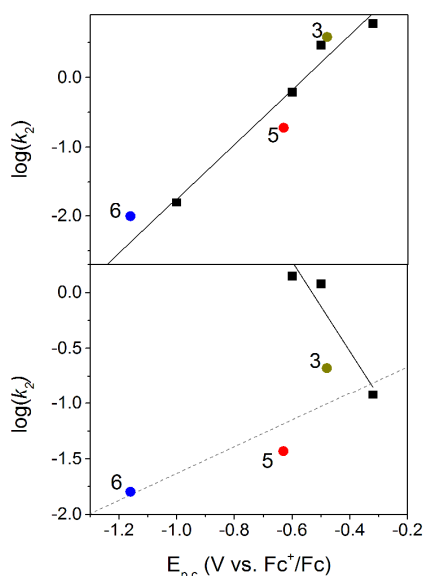

Fig. 10 Correlation of rate constants for OAT (PPh$_3$, top) and HAT (1,4-cyclohexadiene, bottom) reactions with E$_{p,c}$ values of various [Fe^{IV}(O)(TMC)(X)] complexes. Filled circles represent data obtained in this study. Squares represent data from ref. 18 and the solid lines are trend lines created using only this data. The dashed line is the trend line created using the data collected for the complexes in this study plus that for **1-CH$_3$CN**.

to the oxo group was pyridine N-oxide;[15] variation of the 4-substituent on the pyridine N-oxde showed higher HAT reactivity for the more electron donating substituents. This counter-intuitive trend has been accounted for by Shaik and co-workers with a Two-State Reactivity (TSR) model.[22, 23] This model recognizes the proximity of an excited $S = 2$ state that is much more reactive for HAT than the ground $S = 1$ state. As C–H bond cleavage progresses, the reaction coordinate will cross over from the ground triplet surface to the more reactive quintet surface, with an earlier transition being more favorable for HAT. Thus the reactivity of an $S = 1$ Fe^{IV}=O unit is governed by the size of the triplet-quintet gap and spin-orbit coupling; when the triplet-quintet gap decreases as the axial ligand becomes more basic, the spin-orbit coupling increases. For this **1-X** subset, the parent complex with X = CH$_3$CN becomes more reactive when X is replaced by an anionic ligand (X = O$_2$CCF$_3$, N$_3$, SR); in the case of the complex with X = SR (**9**), HAT from 9,10-

dihydroanthracene was 40-fold faster than for **1**. Contrary to our expectations based on the Sastri results, both **5** and **6** were in fact less reactive than **1**, even though both have lower redox potentials than **1**. The axial enolate ligand of **6** should be of comparable basicity as thiolate based on their $E_{p,c}$ values, but the HAT rate of **6** with CHD as substrate is in fact 7-fold slower than for **1** (Table 3) and is estimated to be two orders of magnitude slower than that for **9**. From the above discussion, as well as studies of HAT reactivity on two other sets of oxoiron(IV) complexes,[46, 47] it is clear that HAT reactivity can be affected by other factors besides TSR; this provides impetus for developing a new theoretical model that can account for the wide difference observed in the reactivity of iron(IV)-oxo complexes, especially those with similar ligand sets.

Conclusions

In this study, we have demonstrated that, in an analogous fashion to the TMC-py ligand, appending a *N,N*-dimethylacetamide donor to the TMC ligand framework overcame any inherent thermodynamic barriers associated with coordination of this neutral donor and favored coordination of **L** as a pentadentate ligand in formation of the iron(II) complex **4**. Furthermore, oxidation of **4** with PhIO yielded the ultra-stable oxoiron(IV) complex **5**, with a half-life of a 5 days at 25 °C that is approximately an order of magnitude longer than that of **1-CH$_3$CN** ($t_{1/2}$ 10 h)[18] and the longest thus far reported for any oxoiron(IV) complex. This stability allowed isolation of crystals suitable for X-ray analysis, with the resultant structure being the first of an oxoiron(IV) complex supported by a ligand containing an oxygen atom donor and only the fifth with a $S = 1$ spin-state.[12-15] Interestingly, treatment of **5** with strong base leads to deprotonation of the methylene group that links the appended donor to the cyclam ring and formation of a second, much less stable, oxoiron(IV) complex [Fe^{IV}(O)(**L-H**)](OTf) (**6**). The latter converts to the former in high yield upon treatment with acid, making **5** and **6** the first example of a conjugate acid-base pair in non-heme oxoiron(IV) chemistry. A particularly notable spectroscopic feature of the enolate-like complex **6** is its blue color, which on the basis of TD-DFT calculations is assigned as a LMCT transition originating from the high energy filled MO of the enolate of the pendant acetamide donor to the vacant β (Fe d_{yz}+O p_y)* orbital. This assignment was corroborated by resonance Raman spectroscopy, wherein resonance enhancement of the ν(Fe=O) feature was observed upon excitation at wavelengths near the LMCT band at 588 nm. (In contrast, near UV excitation was required to observe the ν(Fe=O) features of other nonheme oxoiron(IV) complexes.)

The chemical inertness inferred from the remarkably long half-life of **5** was confirmed by observation of sluggish intermolecular OAT and HAT reactivity, with k_2 values approximately an order of magnitude slower than **1-CH$_3$CN** in reactions with PPh$_3$ and CHD. Interestingly, the significantly less stable complex **6** is an even less facile oxidant than **5** in both OAT and HAT. It is clear that this series of complexes defy the anti-electrophilic trend in HAT reactivity established for the closely related **1-X** series of complexes.[20] Given that the only structural parameters that differ significantly between the DFT optimized geometries of **5** and **6** are those associated with the axial donor, it seems likely that

changes in the basicity of the axial donor alone are not enough to yield enhanced reactivity in HAT. This finding adds another facet to the increasingly complex reaction landscape of $S = 1$ oxoiron(IV) complexes, and serves to highlight the shortcomings of our mechanistic understanding. It is clear that further systematic studies are required in order to unify all mechanistic observations into a single model that will allow qualitative prediction of reactivity of $S = 1$ oxoiron(IV) complexes as a function of supporting ligand.

Acknowledgements

Experimental

Complete experimental and computational methods are provided in the Electronic Supplementary Information.

Notes and references

^{a} Department of Chemistry and Center for Metals in Biocatalysis, University of Minnesota, 207 Pleasant St. SE, Minneapolis, Minnesota 55455, USA. E-mail: larryque@umn.edu
^{b} Department of Chemistry, Carnegie Mellon University, 4400 5th Ave., Pittsburgh, PA 15213, USA. E-mail: emunck@cmu.edu

$^+$Currently at the Max Planck Institute for Chemical Energy Conversion, Stiftstrasse 34-36, D-45470, Mülheim an der Ruhr, Germany.
$^{//}$Current Address: Department of Chemistry, Harvey Mudd College, 301 Platt Blvd, Claremont, California 91711
§ Current Address: Case Center for Synchrtron Biosciences, Brookhaven National Laboratory, Upton, NY 11973

† Electronic Supplementary Information (ESI) available: [Experimental procedures, X-ray crystallographic data, kinetic data, ESI-MS data, additional XAS and electrochemical data, and supplementary DFT information]. See DOI: 10.1039/b000000x/

1. C. Krebs, D. Galonic Fujimori, C. T. Walsh and J. M. Bollinger, Jr., *Acc. Chem. Res.*, 2007, **40**, 484-492.
2. E. G. Kovaleva and J. D. Lipscomb, *Nat. Chem. Biol.*, 2008, **4**, 186-193.
3. J. C. Price, E. W. Barr, B. Tirupati, J. M. Bollinger, Jr. and C. Krebs, *Biochemistry* 2003, **42**, 7497-7508.
4. L. M. Hoffart, E. W. Barr, R. B. Guyer, J. M. Bollinger, Jr. and C. Krebs, *Proc. Natl. Acad. Sci. U.S.A.*, 2006, **103**, 14738-14743.
5. B. E. Eser, E. W. Barr, P. A. Frantom, L. Saleh, J. M. Bollinger, Jr., C. Krebs and P. F. Fitzpatrick, *J. Am. Chem. Soc.*, 2007, **129**, 11334-11335.
6. D. P. Galonic, E. W. Barr, C. T. Walsh, J. M. Bollinger, Jr. and C. Krebs, *Nat. Chem. Biol.*, 2007, **3**, 113-116.
7. M. L. Matthews, C. M. Krest, E. W. Barr, F. H. Vaillancourt, C. T. Walsh, M. T. Green, C. Krebs and J. M. Bollinger, Jr., *Biochemistry* 2009, **48**, 4331-4343.
8. A. J. Panay, M. Lee, C. Krebs, J. M. Bollinger, Jr. and P. F. Fitzpatrick, *Biochemistry*, 2011, **50**, 1928-1933.
9. A. R. McDonald and L. Que, *Coord. Chem. Rev.*, 2013, **257**, 414-428.
10. J. Hohenberger, K. Ray and K. Meyer, *Nat. Commun.*, 2012, **3**, 720.
11. S. P. de Visser, J.-U. Rohde, Y.-M. Lee, J. Cho and W. Nam, *Coord. Chem. Rev.*, 2013, **257**, 381-393.
12. J.-U. Rohde, J.-H. In, M. H. Lim, W. W. Brennessel, M. R. Bukowski, A. Stubna, E. Münck, W. Nam and L. Que, Jr., *Science*, 2003, **299**, 1037-1039.
13. E. J. Klinker, J. Kaizer, W. W. Brennessel, N. L. Woodrum, C. J. Cramer and L. Que, Jr., *Angew. Chem., Int. Ed.*, 2005, **44**, 3690-3694.
14. A. Thibon, J. England, M. Martinho, V. G. Young, J. R. Frisch, R. Guillot, J.-J. Girerd, E. Münck, L. Que, Jr. and F. Banse, *Angew. Chem., Int. Ed.*, 2008, **47**, 7064-7067.
15. S. Meyer, I. Klawitter, S. Demeshko, E. Bill and F. Meyer, *Angew. Chem., Int. Ed.*, 2013, **52**, 901-905.
16. J. England, Y. Guo, R. Farquhar Erik, G. Young Victor, Jr., E. Münck and L. Que, Jr., *J. Am. Chem. Soc.*, 2010, **132**, 8635-8644.
17. D. C. Lacy, R. Gupta, K. L. Stone, J. Greaves, J. W. Ziller, M. P. Hendrich and A. S. Borovik, *J. Am. Chem. Soc.*, 2010, **132**, 12188-12190.
18. J.-U. Rohde and L. Que, Jr., *Angew. Chem., Int. Ed.*, 2005, **44**, 2255-2258.
19. J.-U. Rohde, A. Stubna, E. L. Bominaar, E. Münck, W. Nam and L. Que, Jr., *Inorg. Chem.*, 2006, **45**, 6435-6445.
20. C. V. Sastri, J. Lee, K. Oh, Y. J. Lee, J. Lee, T. A. Jackson, K. Ray, H. Hirao, W. Shin, J. A. Halfen, J. Kim, L. Que, Jr., S. Shaik and W. Nam, *Proc. Natl. Acad. Sci. U. S. A.*, 2007, **104**, 19181.
21. Y. Zhou, X. Shan, R. Mas-Balleste, M. R. Bukowski, A. Stubna, M. Chakrabarti, L. Slominski, J. A. Halfen, E. Münck and L. Que, Jr., *Angew. Chem., Int. Ed.*, 2008, **47**, 1896-1899.
22. H. Hirao, D. Kumar, L. Que, Jr. and S. Shaik, *J. Am. Chem. Soc.*, 2006, **128**, 8590-8606.
23. H. Hirao, L. Que, Jr., W. Nam and S. Shaik, *Chem.--Eur. J.*, 2008, **14**, 1740-1756.
24. S. Shaik, H. Chen and D. Janardanan, *Nat. Chem.*, 2011, **3**, 19-27.
25. D. Usharani, D. Janardanan, C. Li and S. Shaik, *Acc. Chem. Res.*, 2013, **46**, 471-482.
26. M. S. Seo, H. G. Jang, J. Kim and W. Nam, *Bull. Korean Chem. Soc.*, 2005, **26**, 971-974.
27. S. A. Wilson, J. Chen, S. Hong, Y.-M. Lee, M. Clemancey, R. Garcia-Serres, T. Nomura, T. Ogura, J.-M. Latour, B. Hedman, K. O. Hodgson, W. Nam and E. I. Solomon, *J. Am. Chem. Soc.*, 2012, **134**, 11791-11806.
28. C. Bucher, E. Duval, J.-M. Barbe, J.-N. Verpeaux, C. Amatore and R. Guilard, *C. R. l'Academie. Sci., Ser. IIC*, 2000, **3**, 211-222.
29. C. Amatore, J.-M. Barbe, C. Bucher, E. Duval, R. Guilard and J.-N. Verpeaux, *Inorg. Chim. Acta*, 2003, **356**, 267-278.
30. D. Tschudin, A. Basak and T. A. Kaden, *Helv. Chim. Acta*, 1988, **71**, 100-106.
31. D. Tschudin and T. A. Kaden, *Pure Appl. Chem.*, 1988, **60**, 489-493.
32. T. A. Kaden, D. Tschudin, M. Studer and U. Brunner, *Pure Appl. Chem.*, 1989, **61**, 879-883.
33. A. W. Addison, T. N. Rao, J. Reedijk, J. Van Rijn and G. C. Verschoor, *J. Chem. Soc., Dalton Trans.*, 1984, 1349-1356.
34. E. K. Barefield, *Coord. Chem. Rev.*, 2010, **254**, 1607-1627.

35. T. A. Jackson, J.-U. Rohde, M. S. Seo, C. V. Sastri, R. DeHont, A. Stubna, T. Ohta, T. Kitagawa, E. Münck, W. Nam and L. Que, Jr., *J. Am. Chem. Soc.*, 2008, **130**, 12394-12407.

36. A. Decker, J.-U. Rohde, L. Que, Jr. and E. I. Solomon, *J. Am. Chem. Soc.*, 2004, **126**, 5378-5379.

37. A. Decker, J.-U. Rohde, E. J. Klinker, S. D. Wong, L. Que, Jr. and E. I. Solomon, *J. Am. Chem. Soc.*, 2007, **129**, 15983-15996.

38. J. Kaizer, E. J. Klinker, N. Y. Oh, J.-U. Rohde, W. J. Song, A. Stubna, J. Kim, E. Münck, W. Nam and L. Que, Jr., *J. Am. Chem. Soc.*, 2004, **126**, 472-473.

39. F. H. Allen, O. Kennard, D. G. Watson, L. Brammer, A. G. Orpen and R. Taylor, *J. Chem. Soc., Perkin Trans. 2*, 1987, S1-S19.

40. L. G. Wade, *Organic Chemistry*, Pearson Prentice Hall, Upper Saddle River, NJ, 2006.

41. F. A. Carey, *Organic Chemistry*, McGraw Hill, New York, 2006.

42. K. Ray, J. England, A. T. Fiedler, M. Martinho, E. Münck and L. Que, Jr., *Angew. Chem., Int. Ed.*, 2008, **47**, 8068-8071.

43. L. Toib, S. Dermaik, M. Michman and Y. Sasson, *Synlett*, 1995, 245-246.

44. J.-U. Rohde, S. Torelli, X. Shan, M. H. Lim, E. J. Klinker, J. Kaizer, K. Chen, W. Nam and L. Que, Jr., *J. Am. Chem. Soc.*, 2004, **126**, 16750-16761.

45. M. R. Bukowski, K. D. Koehntop, A. Stubna, E. L. Bominaar, J. A. Halfen, E. Münck, W. Nam and L. Que, Jr., *Science*, 2005, **310**, 1000-1002.

46. D. Wang, K. Ray, M. J. Collins, E. R. Farquhar, J. R. Frisch, L. Gomez, T. A. Jackson, M. Kerscher, A. Waleska, P. Comba, M. Costas and L. Que, Jr., *Chem. Sci.*, 2013, **4**, 282-291.

47. S. Hong, Y.-M. Lee, K.-B. Cho, K. Sundaravel, J. Cho, M. J. Kim, W. Shin and W. Nam, *J. Am. Chem. Soc.*, 2011, **133**, 11876-11879.

We report the first conjugate acid-base pair of nonheme oxoiron(IV) complexes, which are supported by a tetramethylcyclam ligand with a pendant amide that binds to the oxo group.